ECOSYSTEMS

Spatial Signatures of Biological Soil Crusts and Community Level Self-organization in Drylands

Daniel Kozar,[1]* Bettina Weber,[2] Yu Zhang,[3] and Xiaoli Dong[1]

[1]Department of Environmental Science and Policy, University of California, Davis, California 95616, USA; [2]Institute for Biology, University of Graz, Holteigasse 6, 8010 Graz, Austria; [3]Earth and Environmental Sciences Division, Los Alamos National Laboratory, Los Alamos, New Mexico 87545, USA

ABSTRACT

While vascular plants in drylands can spatially self-organize and persist under climatic stress through gradual changes in patch attributes, dryland patch dynamics largely assumes bare soil between plants. Biological soil crusts (BSCs) are communities living in the soil surface of drylands and mediate water redistribution in space. BSCs often occur in patches of light cyanobacteria and dark-mixed aggregates; however, little is known about their spatial patterns and dynamics. Here, we investigate spatial attributes of BSC patches, their spatial interactions with vascular plants, and factors that drive variation in these attributes using ultra-high-resolution (1 cm) maps from UAV imagery across three ecoregions of the southwest United States. Our analysis showed that light cyanobacteria BSCs varied most in patch shape complexity with aridity, while dark-mixed BSCs varied most in abundance. The distribution of dark-mixed BSCs was strongly affected by the soil template (texture and calcareousness) and vascular plants. Light cyanobacteria BSCs and woody plants spatially aggregated with aridity, while slope enhanced the spatial association between BSC functional groups. We conclude that light cyanobacteria BSCs can likely persist under stress through patch shape alterations, while dark-mixed BSC patches may have a lower capacity to do so—corroborating that dark-mixed BSC abundance may decline under altered climatic regimes. Light cyanobacteria BSCs may also buffer the effects of aridity for other biota by promoting runoff. BSCs and vascular plants coordinate in space in response to resource availability, suggesting the need to consider self-organization of multiple unique assemblages to better predict dryland response to climate change.

Key words: patch dynamics; ecohydrology; spatial feedbacks; aridification; cryptogams; remote sensing.

Author contributions: D.K., X.D., and B.W. conceived the study and methods. D.K. collected observational data and performed analysis with assistance of X.D and Y.Z. All authors discussed results. D.K. wrote the manuscript with the input of X.D., B.W., and Y.Z. All authors contributed to revisions and writing of the final manuscript.

*Corresponding author; e-mail: djkozar@ucdavis.edu

HIGHLIGHTS

- Light cyanobacteria BSCs persist under stress through changes in patch traits
- Patch dynamics driven by light cyanobacteria BSCs may increase dryland resilience
- Spatial self-organization in drylands is likely a community-level process

INTRODUCTION

Drylands cover approximately 40% of the Earth's terrestrial surface, are home to roughly an equal proportion of the human population and play key roles in regulating global hydrologic and nutrient cycling (Maestre and others 2021). As drylands are defined by water limitation, climatic variation can cause substantial ecosystem response in these landscapes, and the transition from a productive state to one of bare soil under increased stress may be abrupt (D'Odorico and others 2007; Berdugo and others 2020). As many drylands are projected to experience increased climatic stress in the future (Cook and others 2020; Lian and others 2021), understanding complex ecological responses in these landscapes is key to estimate risk of aridification and maximize management effectiveness (Wang and others 2015).

Water scarcity in drylands limits the abundance of vegetation, generating a spatial patchiness pervasive to drylands worldwide (von Hardenberg and others 2010; Okin and others 2015; Eldridge and others 2021). However, through ecohydrological feedbacks, patches of vegetation may also persist at the same cover through alteration of patch attributes (for example, shape, orientation, spatial configuration), rather than size, in response to water limitation (Rietkerk and others 2004; Scheffer 2009; Deblauwe and others 2012). An increase in connectivity of bare space between vegetation patches as a response to reduced abundance may in turn promote vegetative growth in favorable microsites through increased runoff (Mayor and others 2019). The patch attributes of vegetation may therefore change over time such that these vegetative patches receive the same amount of runoff under increased aridity, allowing the ecosystem to maintain productivity within a range of aridity change. Through such ecohydrological feedbacks and patch dynamics, dryland vegetation often self-organizes at large spatial scales—likely increasing ecosystem resilience (van de Koppel and Rietkerk 2004; Bastiaansen and others 2018; Rietkerk and others 2021). As a result, vegetation patches typically become more complex, or less compact, with stress (Aguiar and Sala 1999). On hillslopes, self-organized vegetation patches also tend to orient perpendicular to prevailing slope where runoff from interspaces is most readily available (Deblauwe and others 2012). Spatial self-organization is an important process that allows sessile organisms to persist in harsh environments, and in drylands, spatial feedbacks mediated by the redistribution of rainfall as runoff by different types of patches play a critical role.

The dominant paradigm of dryland patch dynamics considers only two types of patches, bare soil and vascular plants (Rietkerk and others 2004, 2021; Bastiaansen and others 2018). However, soil between vascular plant patches is often abundant with biota living in the soil surface (Bowker and others 2018). Biological soil crusts (hereafter BSCs) are complex, largely autotrophic, communities living in the soil surface of drylands between patches of vegetation (Bowker and others 2013, 2018; Belnap and others 2016; Chamizo and others 2016). These poikilohydric communities often cover more proportional area than vascular plants and play key ecosystem roles through their effects on hydrologic cycling (Bowker and others 2013; Chamizo and others 2016; Eldridge and others 2020, 2021), nitrogen fixation (Barger and others 2013, 2016; Weber and others 2015), and soil stabilization (Williams and others 2012; Belnap and Büdel 2016). In BSCs, filamentous cyanobacteria colonize and stabilize the soil surface via the excretion of exopolysaccharides (EPS) (Colica and others 2014; Büdel and others 2016; Kidron and others 2020, 2022), which promotes the immigration of species with greater water requirements, like dark N-fixing cyanobacteria, lichens, and bryophytes (Belnap and others 2008; Büdel and others 2016; Muñoz-Martín and others 2019; Cantón and others 2020). While relative abundance, composition, and structure of BSCs vary, they typically form two distinct groups—lightly pigmented cyanobacteria, hereafter light cyanobacteria, and darker aggregated patches of N-fixing cyanobacteria, bryophytes, and lichens, hereafter dark-mixed BSCs (Chamizo and others 2012b; Maier and others 2018; Eldridge and others 2020; Havrilla and others 2020; McIntyre and others 2021). These patches of dark-mixed BSCs are typically very diverse, often with several species present within a few square centimeters. Likely owing to lower water requirements and relatively high lateral expansion rates of light cyanobacteria patches, these BSCs often predominate at high levels of abiotic stress compared to dark-mixed BSCs (Read and others 2016; Sorochkina and others 2018; Tamm and others 2018; Becerra-Absalón and others 2019). Dark-mixed BSC cover has been observed to decrease, sometimes rapidly, in response to increased abiotic stress (Maestre and others 2015; Ferrenberg and others 2015). Therefore, patches of these BSC groups may have contrasting capacities to adjust shape through regeneration and

persist under water limitation—with dark-mixed BSCs likely having a lower capacity to do so.

Spatial patterns in drylands are appreciably shaped by ecohydrological interactions between BSCs and vascular plants (Kidron 2007, 2019; Zhang and others 2016; Havrilla and others 2019; Eldridge and others 2020, 2021). Light cyanobacteria BSCs are smooth and often promote runoff—likely concentrating water in sink patches of vascular plants and dark-mixed BSCs (Eldridge and others 2000; Yair 2001; Rodríguez-Caballero and others 2012; Read and others 2016; Kidron and others 2020). While the morphological structure and diversity of dark-mixed BSC patches vary, these well-developed crusts increase surface roughness and typically promote pooling and interception of runoff relative to light cyanobacteria BSCs (Kidron 2007, 2019; Chamizo and others 2016; Guan and Liu 2019). Vascular plants have varying effects on BSCs as they can locally inhibit cyanobacterial growth by deposition of leaf litter (Zhang and others 2016; Lan and others 2021), but also promote dark-mixed patches by providing local shading and high soil moisture (Bowker and others 2016; Navas Romero and others 2020). These coupled interactions between patches of dryland functional groups likely feedback to affect the redistribution of water in drylands (Amir and others 2022). As such, to understand the spatial patterns of vegetation in drylands and their changes, it is necessary to consider spatial self-organization of multiple interacting groups, that is, spatial self-organization at the community level beyond the existing theory focused on a single homogenous group.

BSCs, together with vascular plants, form a spatially distributed community and likely organize in space as a response to abiotic stress and local mediation of that stress, creating a dynamic matrix of biota in dryland landscapes. Despite recent developments in mapping BSCs in space with remote sensing technology (Weber and Hill 2016; Rodríguez-Caballero and others 2017; Rozenstein and Adamowski 2017; Havrilla and others 2020), little has been done to understand patch dynamics of BSCs and underlying processes driving variations in their patch attributes. In this study, we mapped BSCs at 26 sites across the southwest United States, quantified their patch attributes along the aridity gradient as well as spatial interactions between patches of different functional groups, and lastly, we assessed effects of climatic and environmental drivers on patch attributes and interactions.

METHODS

Field Data Collection

Sites Description

To characterize BSC patches and investigate likely drivers of variation in their characteristics, we selected 26 sites across three ecoregions of drylands in the southwest United States—the Great Basin (9 sites), the Colorado Plateau (9 sites), and the Mojave Desert (8 sites) (Figure 1; Table S1). These three dryland ecoregions make for an ideal study system as they provide substantial variation in environmental and climatic conditions. The Great Basin is a cold desert with frost-heaving and deep soil profiles (Snyder and others 2019). The Colorado Plateau is also a cold desert with sedimentary soils (Duniway and others 2016). The Mojave is a hot rain shadow desert characterized by high aridity and nutrient poor alluvial deposits (Thorne 1986). The 26 sites were chosen to cover broad variation in climate, soil, and topography. Within each ecoregion, a smaller subregion was first identified to provide a substantial gradient in aridity within a relatively small area, with a total limit of distance between furthest sites set at 100 miles. Within each smaller subregion, we chose study sites to provide large variation in topography, soil type, and texture. All sites are on property of the United States Bureau of Land Management (BLM), which allots grazing—allowing analysis of the effects of this disturbance. Annual climatic water deficit (CWD), a measure of aridity equal to the depth of evaporative demand that exceeds rainfall, ranges between 912 and 1887 mm yr^{-1} across sites. Minimum and maximum temperature range from -22 to -4 °C and 36–48 °C, respectively. Elevation ranges from 210 to 1850 m. Mean site slope varies between 0° and 3.6°, while hillslope aspect includes north and south facing slopes ranging from 0° to 357°. Soil texture at these sites ranges from silty clay loam to sandy loam.

Community Mapping and Ground Truthing

To map the spatial pattern of BSC-vascular plant communities at each site, we collected 1 cm resolution visible spectrum (RGB) unmanned aerial vehicle (UAV) imagery at all sites in a 50 m by 50 m plot using a DJI Phantom 4 Pro V2.0 at a flight height of 120 feet. UAV flights were conducted from August 16 to August 31, 2021, between 10:00 and 15:00 to limit shadow cover. We selected these dates to maximize desiccation of BSCs and limit photosynthetic similarity between
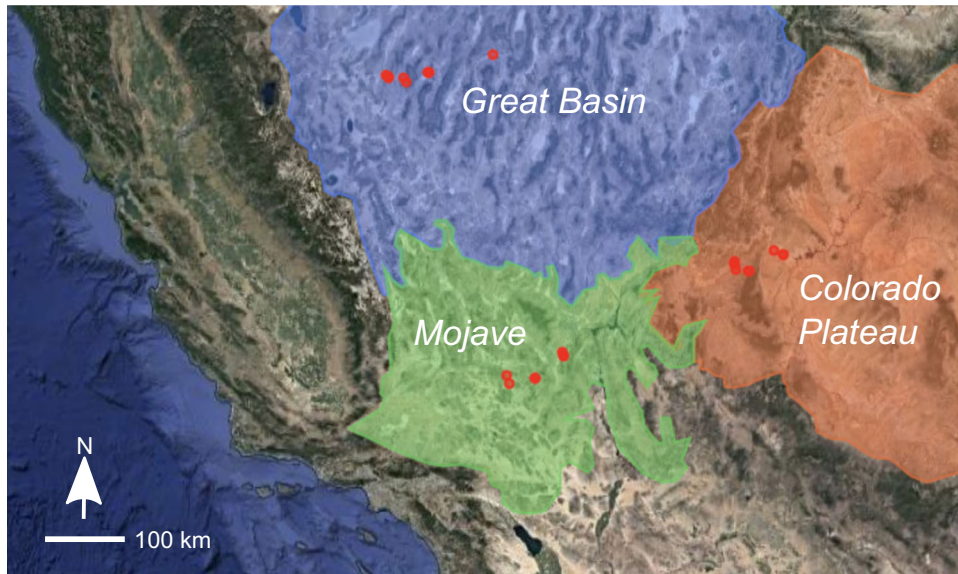
Figure 1. Locations of 26 study sites (red markers) within approximate boundaries of each of the three ecoregions included in this study: the Great Basin, Mojave Desert, and Colorado Plateau. Sites within each region vary by aridity, slope, aspect, and soil conditions. Base imagery: Gorelick and others (2017).

them and vascular plants. Collected images were first orthorectified using the photogrammetry software Agisoft Metashape (2021). Orthorectified images were then classified using a maximum likelihood classifier in ENVI version 5.5 (Exelis Visual Information Solutions 2022).

We considered a total of eight classes in spectral classification: light cyanobacteria BSC, dark-mixed BSC, woody vegetation, herbaceous vegetation, rock, shadow, non-photosynthetic vegetation (leaf litter and woody debris), and bare soil. Spectrally unique subclasses were considered, namely uniquely colored lichens within dark-mixed BSC patches. All spectral subclasses were combined prior to spatial analysis. 50 ground truthing points were chosen for each class and subclass present to inform the maximum likelihood classifier, often resulting in 100 or more ground truthing points for classes with multiple subclasses. 70% of ground truthing points were used for training the classifier, while 30% were used out-of-sample for cross-validation. These ground truthing points were informed from twelve 25 cm by 25 cm quadrats at each site. These quadrats were selectively placed to prioritize the inclusion of multiple classes per quadrat and distributed around sites at least several meters apart to representatively capture spectral variation of classes across quadrats (Figure S1). While most ground truthing data were selected from within quadrats, some data were selected from outside of these quadrats, typically near quadrats and informed from notes and images from

sites, to further increase independence and representativeness of ground truthing data. Large, easily identifiable, woody vegetation patches and shadows were not included in quadrats and were identified by images and notes taken at each site. Although dead plant patches of only woody debris (here considered non-photosynthetic vegetation) may provide some shade to BSCs, these instances were uncommon and are not expected to significantly affect our results of spatial association. We identified BSC patches and constituent species using a BSC specific field guide (Rosentreter and others 2007). Common bryophyte species across ecoregions included *Bryum argenteum, Syntrichia caninervis* and *Syntrichia ruralis*. Common lichen species across ecoregions included *Placynthiella spp., Fulgensia desertorum* and *Placidium squamulosum*. More diverse and sometimes uniquely colored taxa of lichens, largely found in less arid regions of the Great Basin and Colorado Plateau, included *Psora cerebriformis, Psora decipiens, Candelariella citrina, Acarospora nodulosa,* and *Squamarina lentigera*. We distinguished between bare soil and light cyanobacteria BSCs by taking samples of the top crusted layer across at least 10 transects between vascular plant patches, where no loose soil was present, and identifying evidence of EPS, which suspends soil particles from the main crusted layer (Lange and Belnap 2016). Where EPS were present, we considered that type of patch as light cyanobacteria while loose soil or physical crusts were classified as bare soils. While some BSCs,

typically dark-mixed patches, may grow directly beneath the canopy of woody plants and be obscured in aerial imagery (Zhang and others 2016), these patches often extend beyond the canopy's reach at our sites, even in highly arid environments.

To test the expectation that BSCs fall into two classes in the visible spectrum (Havrilla and others 2020), the number of spectral classes (groups) of BSCs in our study was first evaluated by K-means silhouette analysis of three 3 m by 3 m subplots at one site within each ecoregion (Figure S2). Subplots were chosen to provide near complete BSC cover and a representative gradient of BSC development. Silhouette analysis identifies the number of spectral classes with the greatest separation distance between them using an unsupervised classification scheme (Shutaywi and Kachouie 2021). Spectra of BSCs in all ecoregions showed greatest divergence when BSCs fell into two types in our data (Figure S2). While we were unable to relate species-level composition to the two spectral classes in our imagery, this suggests that these soil communities in our study area are constituted of spectrally distinct patches of light cyanobacteria and dark-mixed aggregates.

Classification accuracies were assessed with Cohen's kappa (k) coefficient, an overall conservative measure of accuracy across classes (Fitzgerald and Lees 1994), with a minimum k of 0.75 to be included in analysis. We set this cutoff to limit the effects of classification error on patch metric calculations and further analysis. We were able to obtain k greater than or equal to this cutoff at 22 of the total 26 sites (Figures S3, S4 and S5)—leaving four sites out of the rest of our analysis. High classification errors at these four sites are likely caused by high photosynthetic similarity between BSCs and vascular plants, spectral similarity between light cyanobacteria and bare soil, and movement of ground level objects by high winds.

Soil Sampling

We collected three soil samples of the top 5 cm of soil (Barger and others 2013; Havrilla and Barger 2018) using a 1 ½'' diameter galvanized steel pipe along 25 m intervals at each site. For all soil samples containing BSCs, the top crusted layer was separated from the underlying soil to isolate soil substrate. We then evaluated all soil substrate samples for texture, calcareousness (% as $CaCO_3$), and total nitrogen (nitrogen) (%)—all considered to appreciably affect the composition and abundance of the BSC community (Bryce and others

2012; Bowker and others 2016). Soil texture was calculated through the sedimentation method in 100-mL graduated cylinders (Taubner and others 2009). To validate these measurements, we randomly selected ten soil samples and analyzed soil texture using density analysis (Sheldrick and Wang 1993). We find that these two methods provide statistically similar results (Figure S6). Soil calcareousness and nitrogen content were obtained through gravimetric loss (U.S. Salinity Laboratory Staff 1954) and combustion methods (AOAC Official Method 972.43 1997), respectively. Soil calcareousness and nitrogen content quantification, as well as the soil texture measurements using density analysis, were all carried out by the UC Davis Analytical Lab.

Data Analysis and Statistical Modeling

Analyses of Spatial Patterns and Principal Components

To characterize the spatial attributes of BSC patches, including both light cyanobacteria and dark-mixed BSCs, we calculated a total of 17 spatial metrics using *landscapemetrics* in R (Hesselbarth and others 2019) for each BSC group using classified imagery. These 17 metrics quantify patch abundance, patch shape complexity, dominance, edge effects, and aggregation (Table 1). To identify the aspects of spatial patterns that capture the most variation in all 17 metrics across sites, we paired principal component analysis (PCA) with linear regression of metric data (Larson and Funk 2016). PCA reduces data dimensionality by calculating principal component values (PCs) for each site across various metrics, which capture variation in the data with fewer variables (Demšar and others 2013).

To ensure that our characterization of BSC spatial attributes is robust to the spatial resolution of aerial imagery and the possibility of spurious isolated pixels of classes, we reduced the resolution of our classified data to 2 cm, half that of the original data, and repeated the PCA procedure using the same 17 metrics at each site for each BSC group. To obtain BSC patches at this reduced resolution, new cells were assigned values over a 4 cm^2 sampling grid (four original cells) in the existing classification raster. If a BSC group occupied less than half of the original cells, the new cell was classified as not occupied by that BSC group. If a BSC group occupied half or more of the four original cells within a new sampling grid cell, that new cell was classified as that BSC. If BSC groups occupied equal proportions of the four original cells, we assigned the BSC group of the new classification randomly.

Table 1. Spatial Metrics for PCA Calculated for Each BSC Patch Type

Metric	Unit	Description
Edge density	m ha^{-1}	Edge of a class per unit area, measure of complexity
Perimeter–area (P-A) ratio	–	Ratio of patch perimeter to area, measure of complexity
Coefficient of variation P-A ratio	–	Measure of variance in patch P-A ratio, variation in complexity
Aggregation	%	Measure of aggregation of a patch type
Proportional cover	–	Measure of total abundance
Number of patches	–	Number of unique patches, measure of abundance
Mean patch area	ha	Average patch area
Clumpiness	–	Measure of aggregation of a patch type
Cohesion	%	Connectivity-based measure of aggregation of a patch type
Division	%	Measure of aggregation of a patch type
Mean fractal dimension	–	Mean patch fractal dimension, measure of complexity across scales
Interspersion and juxtaposition index (IJI)	%	Measure of intermixing and aggregation of a patch type
Largest patch index (LPI)	%	Percent area of largest patch, measure of dominance
Landscape shape index (LSI)	–	Measure of aggregation of a patch type
Patch density	ha^{-1}	Number of patches per unit area, measure of abundance
Percent like adjacency (PLADJ)	%	Measure of aggregation of a patch type
Edge length	m	Total length of class edge in landscape, measure of complexity

Using these new reduced resolution classifications, we then evaluated PCs of the same 17 metrics.

To further examine the robustness of our classification approach, we compared area (cm^2), perimeter (cm), and fractal dimension (−), a scale invariant measure of complexity, between patches generated from our classifications and observed patches in orthomosaics. We compared these metrics for 4 randomly selected patches of each BSC class at the site of Colorado Plateau 9 (CP 9). Observed patches were rasterized hand drawn patches that were identified and traced in the orthomosaic without viewing the classification a priori. While light cyanobacteria patch area was less than the observed patches ($\sim$ 30%) across patches, we found that patch metrics of area, perimeter, and complexity between the classification and visually identified patches were similar (Figure S7).

Patch Orientation

To characterize site-level patch orientation of BSCs, a potential outcome of ecohydrological processes on patch dynamics on hillslopes (Deblauwe and others 2011, 2012), we evaluated the directional connectivity index (DCI) (Larsen and others 2012) for each BSC group at each site. DCI determines the connectivity of a patch class or group, across all patches, at a given angle within a classified matrix (Larsen and others 2012). We calculated DCI between 0° and 90° from north at 10° intervals to capture all directional variation. With calculated DCI for a given group, we then computed the difference between angle of maximum DCI and angle of prevailing slope face of a given site, $\Delta\theta$ (°). As such, $\Delta\theta$ is approximately 90° when patch dominant orientation is perpendicular to the prevailing slope, suggesting the capacity for patches to capture surface runoff through gradual adjustments in shape (Deblauwe and others 2012). However, $\Delta\theta$ for BSCs likely deviates somewhat from 90° due to microtopography within sites (Rodríguez-Caballero and others 2019) and environmental stochasticity. Therefore, we set 60° as a critical threshold for $\Delta\theta$ to be approximately perpendicular to hillslope in our analysis. We also expect that $\Delta\theta$ is affected by landscape slope.

Spatial Interactions Within Dryland Communities

To characterize the type (positive *vs.* negative) and strength of ecological interaction between dryland functional groups, we calculated the mean spatial interaction, $X_{i\text{-}j}$, between each BSC type and woody vegetation. These interactions include between light cyanobacteria BSCs and woody vegetation, dark-mixed BSCs and woody vegetation, as well as light cyanobacteria and dark-mixed BSCs. While BSCs interact with herbaceous plants as well, this biotic group was considerably present at only 6 of all 22 sites included in analysis. We calculated $X_{i\text{-}j}$, the spatial interaction between groups i and j, via the spatial analysis through distance indices (SADIE) method developed by Perry 1998. X_{i-j} is calculated through deriving local spatial interaction from clustering maps (equation 1) (Perry and Dixon 2002):

$$X_{i-j,k} = \frac{n(v_{i,k} - \bar{v}_i)(v_{j,k} - \bar{v}_j)}{\sqrt{\sum_k (v_{i,k} - \bar{v}_i)^2 (v_{j,k} - \bar{v}_j)^2}} \quad (1)$$

where $v_{i,k}$ and $v_{j,k}$ are Perry's clustering indices (−) (Perry 1998, Perry and others 1999) of groups i and j in cell k of a 1 m^2 sampling grid (Navas Romero and others 2020), and $\bar{v}_i$ and $\bar{v}_j$ are the mean values of those clustering indices for groups i and j across all sampling grid cells. Perry's clustering index v of a group in k, a unitless metric, is the contribution of k to the overall distance to regularity in a sampled abundance grid using proportional cover within each sampling grid cell—the minimum distance that individuals would have to move to obtain an equal abundance across the entire sampling grid (Perry and Dixon 2002). $X_{i-j,k}$ is the interaction strength between i and j in k, and n is the number of cells within the 1 m^2 sampling grid ($n = 2500$). Local interaction $X_{i-j,\ k}$ is increased if both focal groups have v in k greater than or less than the average of the sampling grid, $\bar{v}$; and $X_{i-j,\ k}$ is decreased if they deviate from the mean in opposite directions. The numerator of $X_{i-j,\ k}$ is normalized through the product of standard deviations of v for groups i and j in the denominator of equation 1. We calculated a site-specific X_{i-j} as the mean of $X_{i-j,\ k}$ across all sampling grid cells within a site (Perry and Dixon 2002).

X_{i-j} is particularly useful in this study as it is standardized to variation in abundance among sites, which allows for comparison of interactions across sites (Perry and Dixon 2002; Navas Romero and others 2020). $X_{i-j} > 0$ indicates positive spatial associations and suggests positive ecological interactions. For example, positive species interactions can result from increased spatial proximity between woody vegetation and dark-mixed BSCs, when vascular plants increase shading for dark-mixed BSCs and dark-mixed BSCs may increase infiltration for those plants (Bowker and others 2016). $X_{i-j} < 0$ indicates negative spatial associations and suggests negative ecological interactions. Competition for water or light between groups, such as burial of light cyanobacteria BSCs by litter of woody vegetation, likely increases spatial segregation of these groups (Zhang and others 2016; Lan and others 2021).

Bayesian Statistical Models

To investigate the driving forces of variation in principle spatial attributes of BSC patches, determined from PCA described above, we used a Bayesian multivariate multiple regression. Outcome variables in this model include the first two PCs of each type of BSC patch, light cyanobacteria and dark-mixed BSCs, making four outcome variables in total. Only the first two PCs were used as these two components capture a majority of total variance in spatial metrics, that is, > 65% for both BSC groups across 17 total metrics (Results). For any PCs which exhibited significant negative relationships to associated spatial metrics, we corrected these PCs in statistical analysis by taking the negative values for ease of direct interpretation of effect size. As we expect these four outcome variables might be correlated, we used a multivariate normal distribution for the likelihood function of the model (equations 2–5) to infer posterior distributions of predictor effect sizes on each outcome:

$$O_i \sim \text{MultivariateNormal}(\mu_i, \mathbf{S}) \quad (2)$$

$$\mu_i = \sum_x \beta_x x_i + \alpha_{\text{region}_i} \quad (3)$$

$$\mathbf{S} = \begin{pmatrix} \sigma_1 \cdots 0 \\ \vdots \ddots \vdots \\ 0 \cdots \sigma_n \end{pmatrix} \mathbf{R} \begin{pmatrix} \sigma_1 \cdots 0 \\ \vdots \ddots \vdots \\ 0 \cdots \sigma_n \end{pmatrix} \quad (4)$$

$$\mathbf{R} \sim LKJ(\eta) \quad (5)$$

where n is the number of outcome variables (O) in the model—$n = 4$ in this case. β_x is the slope parameter describing the effect size of the corresponding predictor variable x, including aridity, slope, aspect, grazing, soil texture, soil CaCO$_3$, and soil nitrogen across all sites (equation 3). Aridity is represented in our model by climatic water deficit (CWD) (mm yr^{-1}) from the TerraClimate dataset, taken as the mean annual value over the past five years (Abatzoglou and others 2018). CWD describes water stress through estimation of the total depth of evaporative demand which exceeds available rainfall, with greater values associated with greater aridity. Slope (°) and aspect (°) were extracted from the United States Geological Survey (USGS) 3D Elevation Program (3DEP) dataset (USGS 2022). Geospatial predictor variables in our model are the average value within the bounds of each site, that is, one value for each variable to represent the mean condition of each site. Predictor data for landscape aspect were converted to northness by taking the cosine of aspect values. Soil texture for individual samples within sites was classified using integers 1–12, increasing in coarseness, according to the United States Department of Agriculture (USDA) system through particle size fractionation analysis. The average of three texture sample values are used to represent

soil texture for each site. Soil calcium carbonate content (% as CaCO₃) and nitrogen content (%) are also averages of the three samples collected within each site. As data on degree of grazing are scarce and difficult to measure (Fetzel and others 2017), grazing disturbance is described with a quotient of observed intensity to estimated time since last grazed. This quotient captures the effect of grazing in a continuous variable, as time is expected to reduce the effects of grazing. Grazing intensity at each site was classified 0–3 on a scale of absent—light-moderate—severe based on our visual inspection of grazing evidence for at least 10 patches of vegetation in the field covering the full extent of the site (Petz and others 2014). We define grazing evidence as having signs of foraging of herbaceous plants or woody leaves in a patch along with trampling depressions. Light grazing (''1'') is defined as having few instances of grazing evidence, while moderate grazing (''2'') is defined as having noticeable grazing across more than half of patches, but not all. Severe grazing (''3'') is defined as having noticeable evidence of grazing across all patches. The time from last major grazing disturbance was classified 1–3 from current—recent—non-detectible, based on evidence of trampling. Time from last major grazing was assigned a ''1'' if trampling was recent, with depressions showing little to no recovery or refill of soil. ''2'' was assigned if trampling depressions were present but depressions were somewhat recolonized by BSCs or refilled with soil. ''3'' was assigned if disturbed soil was completely recolonized by BSCs or no depressions were visible. This normalization of grazing intensity by a measure of time is necessary as vegetation may not necessarily recover from intense grazing while BSCs may recover in that time, and it allows us to represent grazing intensity in a continuous variable. Fire disturbance is not accounted for in our analysis as, according to data from the Monitoring Trends in Burn Severity program (Eidenshink and others 2007) and the Bureau of Land Management (pers. communication), none of our study sites have experienced fire since 1980.

Intercept parameters, α, were pooled by region to elucidate local variance in BSC spatial attributes not captured by predictors included in the model. Weak priors were applied to slope parameters β_x and α_{region}. S is a variance–covariance matrix for all outcome variables, O (equation 4). A Lewandowski-Kurowicka-Joe (LKJ) distribution with shape parameter η of 2 was used for a prior distribution for the correlation matrix R (equation 5).

In the model described above, we used PC1 and PC2 of the patch spatial metrics of light cyanobacteria BSCs and dark-mixed BSCs as outcome variables (Sanchez-Martinez and others 2020). To interpret what each PC represents, we systematically examined the spatial metrics in which these PCs capture the most variance by conducting linear regression analysis between variables and considering correlation across all spatial metrics (Larson and Funk 2016). Once we determined the most plausible spatial attribute that each PC captures, we built a separate model that is a variant of the one described above. In this model variant, we replaced the PC values on the left side of equation (outcome variables, O) (equation 2) with the values of those most plausible metrics we identified. We expect the results of these two models to be largely similar.

We developed a second model to investigate factors driving variation in the interactions between BSC groups and with woody vegetation. The structure of this second model is identical to that of the first model described above (equations 2–5), except that the outcome variables are different, reflecting the types of interactions considered. We included three types of interactions as outcome variables in this model—between light cyanobacteria BSCs and woody vegetation, dark-mixed BSCs and woody vegetation, and light cyanobacteria and dark-mixed BSCs. The two multivariate models share the same set of explanatory variables, including aridity, slope, aspect, grazing, soil texture, soil CaCO₃ content, and soil nitrogen content, as described above (that is, the right side of equation 3 stays the same).

All data included in our statistical models were first standardized by z-scoring to promote model sampling efficiency and allow for direct comparison of effect sizes of different predictors.

Posterior distributions of slope and intercept parameters were constructed using 10,000 samples distributed across five chains using Hamiltonian Monte Carlo (HMC) simulation in *Stan* in R (Gelman and others 2015). These distributions were then used to assess mean standardized slope parameters and degree of confidence in nonzero effect of predictor variables. In this study, central 90% credible intervals were used as a critical degree of confidence to determine statistical significance of parameters. Model convergence was evaluated in our study using trace plots to ensure chains mixed and by ensuring $\hat{r} < 1.1$ (Gelman and Shalizi 2013).

RESULTS

Spectral cluster analysis of BSCs in our study suggested that these communities likely fall into two distinct patches—corresponding to light cyanobacteria and dark-mixed BSCs (Figure S2). BSCs were present at all sites in our study, showing significant variation in proportional cover (Figure 2A) as well as patch shape (Figure 2B). Cover of light cyanobacteria BSCs ranged from 6 to 58%, while cover of dark-mixed BSCs ranged between 0 and 63%. Total coverage of BSCs, including both functional groups, ranged between 11 and 90% across sites. While BSCs occupied more than 50% of total site area at only 12 out of 22 sites included in analysis (Figures S2, S3 and S5), we found that BSCs covered more proportional area than vascular vegetation at all but three sites—two of which were in the Mojave Desert, one was in the Colorado Plateau. This suggests our study sites were largely of a mixed BSC-vegetation state (Chen and others 2020). For patches of similar sizes, their shape may vary significantly (Figure 2B). Mean patch

perimeter–area ratio (P-A ratio), a metric describing patch shape complexity, ranged from 1.25 to 1.58 for light cyanobacteria BSCs and 1.30 to 1.54 for dark-mixed BSCs (P-A ratio for individual patches in Figure 2B, left to right, is 1.66, 2.00, and 2.29). Local interactions with woody vegetation were typically negative for light cyanobacteria BSCs (mean interaction strength $\overline{X} = -0.18$ and standard deviation $\sigma_X = 0.21$ across sites) (Figure 2D) and positive for dark-mixed BSCs ($\overline{X} = 0.10$, $\sigma_X = 0.28$ across sites) (Figure 2E). The two groups of BSCs were typically well segregated in space ($\overline{X} = -0.16$, $\sigma_X = 0.26$ across sites) (Figure 2F).

Through analysis of $\Delta\theta$, the difference between angle of maximum DCI and angle of dominant hillslope face at a given site, we found that light cyanobacteria BSC patches tended to orient perpendicular to slope more readily than dark-mixed BSCs (Figure S8A, B). Although $\Delta\theta$ often deviated from 90° for both BSC groups, the distribution of $\Delta\theta$ for light cyanobacteria tended more toward 90°, with $\Delta\theta$ deviating less than 30° from 90° at 10 sites (Figure S8A) and $\Delta\theta$ for dark-mixed BSCs was only
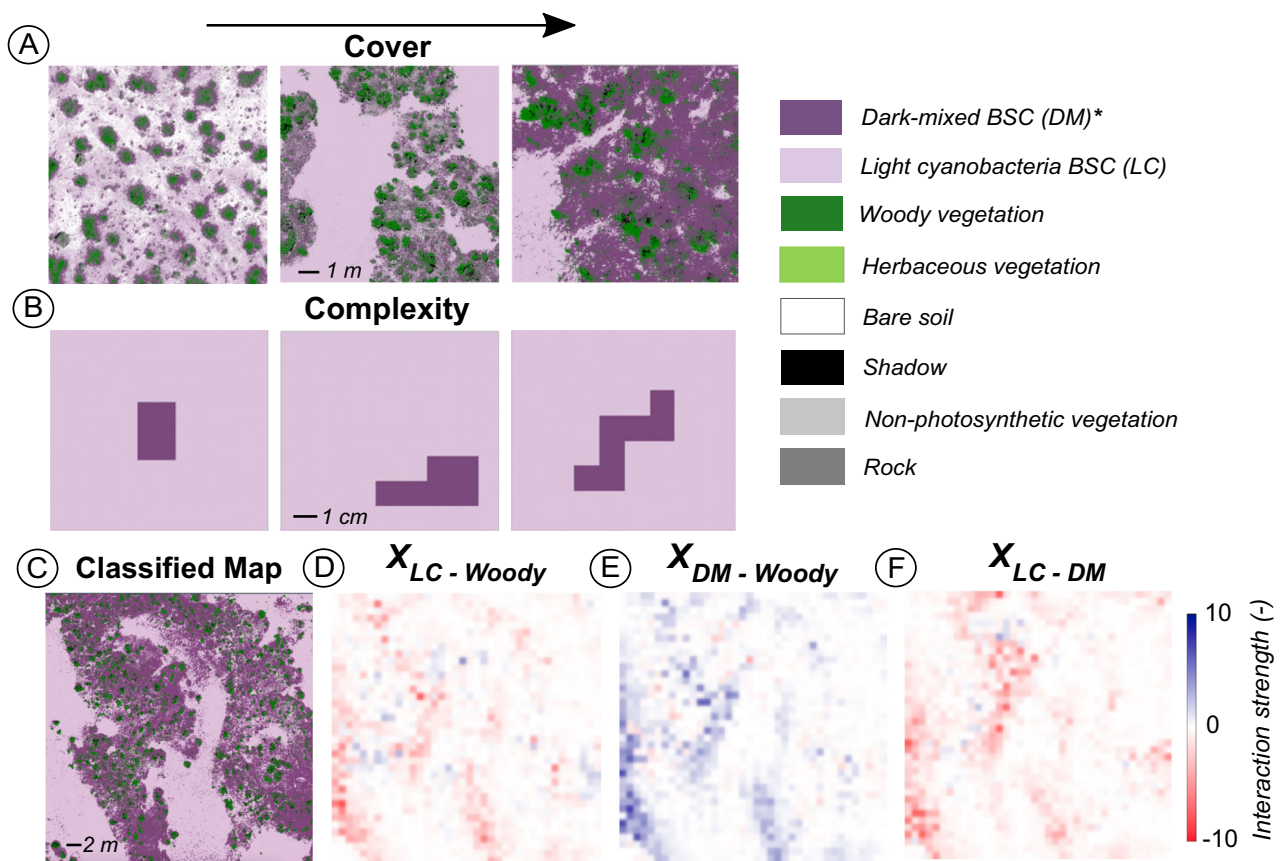

Figure 2. Example classifications displaying variation in **A** abundance and **B** complexity of dark-mixed BSC patches across sites, as well as **C** classified imagery of a site in the Great Basin and **D, E, F** local interactions between woody vegetation and each type of BSC, light cyanobacteria (LC) and dark-mixed (DM) BSCs, within that site.

within 30° deviation from 90° at 5 sites (Figure S8B). Patch orientation of light cyanobacteria BSCs also exhibited greater dependence on slope, as they oriented approximately perpendicular to hillslope at 6 of 8 sites with slope greater than 2° (Figure S8A), compared to only 3 sites for dark-mixed BSCs (Figure S8B).

To further characterize each of the two types of BSC patches, we conducted principal component analysis (PCA) on 17 metrics describing their spatial characteristics (Table 1). The first principal component (PC) of light cyanobacteria BSC patches explained 44.6% of the total variance of 17 metrics across sites, while the second PC explained 29.1% of metric variance (Figure 3A). We found that the first PC was highly correlated with mean perimeter–area ratio ($R^2 = 0.71$, $p = 0.00$) (Figure 3C),

suggesting that this PC captures variation in the complexity of patch shape. The second PC had a significant, high correlation with proportional cover ($R^2 = 0.81$, $p = 0.00$) (Figure 3D), suggesting this PC captures variation in abundance of this BSC type. These results were robust when calculated at a coarser spatial resolution (Figure S9). While the absolute cover of light cyanobacteria might be underpredicted in our classification approach (Figure S7), given that our study focuses on inter-site variations along the aridity gradient, we do not expect that this would significantly affect our PCA results or further analysis. We also found no consistent trend of overprediction or underprediction of light cyanobacteria BSCs across sites (Figures S3, S4 and S5), further suggesting that the PCs of light
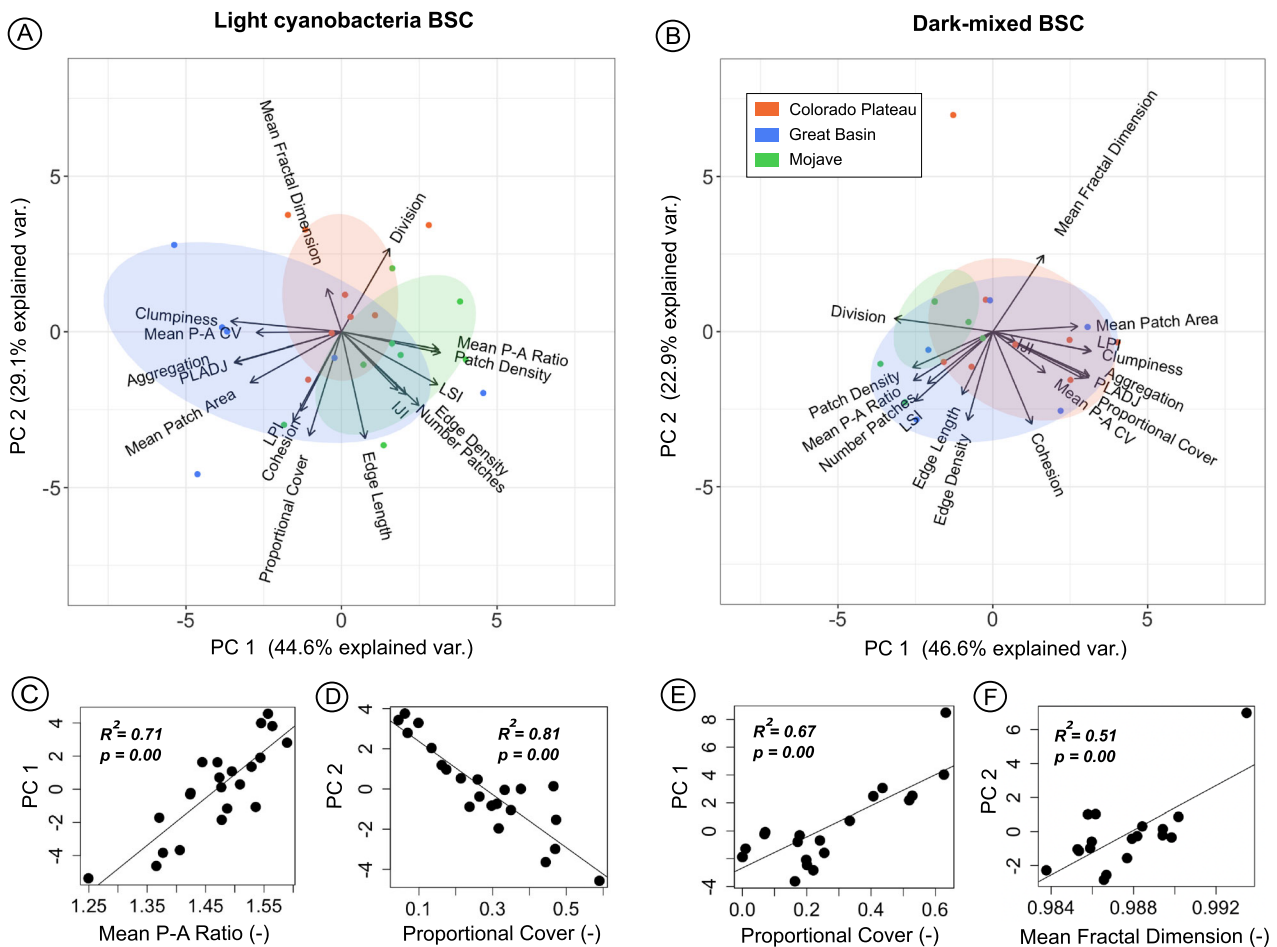

Figure 3. Principal component analysis (PCA) of spatial metrics of BSC patches, showing biplots of the first two principal components (PCs) for **A** light cyanobacteria and **B** dark-mixed BSCs. Site specific values of PCs are grouped in ellipses of 70% confidence by ecoregion. Vectors are shown displaying correlation between spatial metrics and both PCs. The x-component of metric vectors corresponds to correlation with PC1, while correlation of spatial metrics with PC2 comprises the y-component of these vectors. **C, D, E, F** Linear regression plots and correlation coefficients between PCs and spatial metrics suspected to correspond to them.

cyanobacteria BSCs are complexity and cover, respectively.

For dark-mixed BSC patches, PCA showed that the first two PCs of the 17 spatial metrics considered captured 46.6 and 22.9% of the total variance, respectively (Figure 3B). Unlike light cyanobacteria, the first PC of dark-mixed BSC patches was significantly, highly correlated with proportional cover ($R^2 = 0.67$, $p = 0.00$) (Figure 3E) and the second PC was significantly correlated with mean fractal dimension ($R^2 = 0.51$, $p = 0.00$) (Figure 3F)—a scale invariant metric of patch complexity calculated from patch perimeter and area (McGarigal and others 1995; Hesselbarth and others 2019). Additionally, we found that dark-mixed BSCs varied more in overall abundance than light cyanobacteria, as the standard deviation of proportional cover across sites for these two groups was 0.21 and 0.15, respectively. While confusion of dark-mixed BSCs with other classes was limited (Figures S3, S4 and S5), dark-mixed BSCs were most overpredicted in the Great Basin, where they are abundant, possibly increasing the total variance of cover of this group. However, as dark-mixed BSCs are largely absent in high aridity areas, we do not expect for this to affect the PCs of this type of BSC. Like light cyanobacteria BSCs, these results for dark-mixed BSC patch metrics were not significantly changed at a coarser spatial resolution (Figure S9). The first PC of dark-mixed BSCs at coarser resolution was highly correlated with proportional cover ($R^2 = 0.80$, $p = 0.00$) (Figure S9E), while the second PC at 2 cm was significantly correlated with mean fractal dimension ($R^2 = 0.55$, $p = 0.00$) (Figure S9F). While the correlation between the first two PCs and associated dark-mixed BSC attributes was negative at 2 cm resolution, as opposed to positive at 1 cm, these PCs still likely correspond to the same metrics. Magnitudes of site PC values only differed in sign and were highly correlated between the two resolutions (Figure S10). As PCs correspond to eigenvectors of the original metric data, an inverse relationship between PCs and metrics still holds the same interpretation as PCs capture the same amount of variance in metric data, and the eigenvectors to which PCs are projected are merely flipped (Bro and Smilde 2014).

We assessed the strength and significance of environmental predictors on variation in the first two PCs of both types of BSC patches through a Bayesian multivariate multiple regression. Model results suggested a statistically significant positive effect of aridity and slope on patch complexity of light cyanobacteria BSCs (Figure 4A), with mean effect sizes of 0.72 and 0.61, respectively. Grazing also showed a significant positive effect on light cyanobacteria patch complexity, with a mean effect size of 0.44 (Figure 4A). For light cyanobacteria BSC cover, soil coarseness showed a significant positive effect, with a mean effect size of 0.56 (Figure 4B).

No predictors included in our analysis exhibited a statistically significant effect on dark-mixed BSC patch complexity or cover (90% credible interval; Figure 4C, D). Aridity and soil texture (coarseness) displayed the greatest mean effect (both negative) on the first principal component of dark-mixed BSCs, interpreted as total cover (Figure 4C). They were marginally significant within 75 and 80% credible intervals, respectively.

These were results of models using PC values as outcome variables. When we directly used the interpreted metrics that correspond to each PC as model outcomes (for example, replacing PC1 with P-A ratio for light cyanobacteria; Figure 3C), model results stayed largely the same (Figure S11).

To identify the effect of climatic and environmental predictors on variation in interactions between BSC patches and woody vegetation, we specified these interactions as outcome variables in our multivariate regression model. Model results suggested that interactions between BSCs and woody vegetation were significantly affected by aridity, soil texture, and slope. Aridity reduced the degree of spatial segregation ($\overline{X} = -0.18$ across sites) between light cyanobacteria BSCs and woody vegetation (Figure 5A). Soil texture (coarseness) enhanced the typically positive association between dark-mixed BSCs and woody plants ($\overline{X} = 0.10$ across sites) (Figure 5B). Soil calcium carbonate ($CaCO_3$), however, reduced the positive association between dark-mixed BSCs and woody plants (Figure 5B). The only predictor to show a statistically significant effect on the interaction between light cyanobacteria and dark-mixed BSCs, typically negative ($\overline{X} = -0.16$ across sites), was slope, which decreased their spatial segregation (Figure 5C). Aridity also may reduce the spatial segregation between these two groups of BSCs; however, this effect was only marginally significant (Figure 5C).

DISCUSSION

Characteristics and Responses of BSC Spatial Patterns

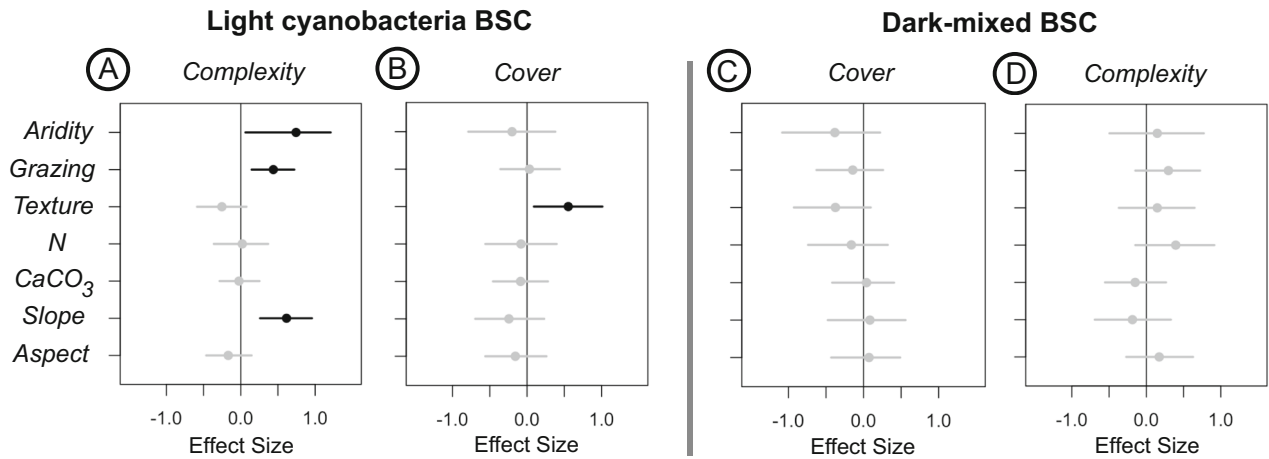When resources become increasingly limited, the abundance of a sessile organism or functional

Light cyanobacteria BSC

Dark-mixed BSC

Figure 4. Posterior distributions of predictor effect sizes on **A** light cyanobacteria BSC PC1 (patch complexity) and **B** PC2 (cover) and **C** dark-mixed BSC PC1 (cover) and **D** PC2 (complexity). Positive effect size means the variable on the y-axis increases the patch complexity (**A** and **D**) or cover (**B** and **C**) of BSCs, while negative effect size denotes negative effects. Mean effect size values are designated by circles and central 90% credible intervals are shown as lines. Parameter distributions statistically different from zero are shown in black, while those that are not significantly different from zero are shown in gray.
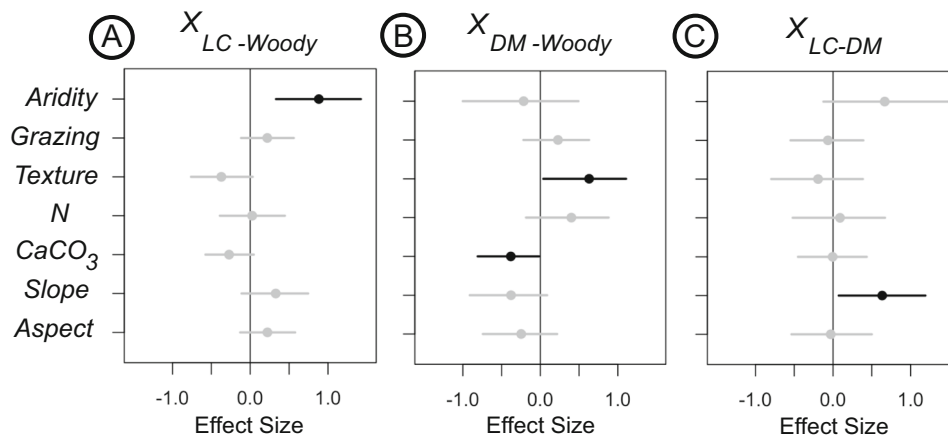

Figure 5. Posterior distributions of predictor effect sizes on the interaction between **A** light cyanobacteria BSCs (LC) and woody vegetation, **B** dark-mixed BSCs (DM) and woody vegetation, and **C** light cyanobacteria (LC) and dark-mixed BSCs (DM). Positive effect size means the variable on the y-axis increases the spatial aggregation (reduces spatial segregation) between groups, and negative effect size means the variable reduces the spatial aggregation (increases spatial segregation) between the two groups. Mean effect size values are designated by circles and central 90% credible intervals are shown as lines. Parameter distributions statistically different from zero are shown in black, while those that are not significantly different from zero are shown in gray.

group will likely decrease (Tilman 1982; Svensson and Marshall 2015). However, a patch of biota may receive the same amount of a resource if new individuals emerge in space to intercept it more readily (Aguiar and Sala 1999). In drylands, vegetation patches often grow in areas where runoff is easily captured, maintaining productivity under high stress (Aguiar and Sala 1999; Couteron and others 2014). Organisms with relatively high stress tolerance and relatively rapid regeneration rates

therefore may be able to maintain their total abundance under greater stress through spatial reorganization. We observed such a response in light cyanobacteria BSC patches. The spatial component of greatest variance for light cyanobacteria along the aridity gradient was patch shape complexity, rather than total cover (Figure 3A,C), and aridity significantly increased light cyanobacteria patch complexity (Figure 4A). We also found evidence that light cyanobacteria BSC patches can

more readily orient perpendicular to prevailing hillslope (Figure S8)—likely a response of patch reorganization (Deblauwe and others 2011). For dark mixed BSCs, which are more sensitive to stress (Reed and others 2012, 2019; Maestre and others 2015; Tamm and others 2018; Ladrón de Guevara and Maestre 2022), the spatial component of greatest variance was cover (Figure 3B, E), which was plausibly negatively affected by aridity (Figure 4C; significant within 75% confidence). While dark-mixed BSCs under the canopy of vegetation possibly not accounted for in our analysis may change patch complexity and increase total cover of this group, especially at sites of low stress, it is unlikely that the PCs of dark-mixed BSCs would change, as this would likely increase total variation in cover across all sites. If dark-mixed BSCs under the canopy of vegetation are considered, we might observe a negative correlation between aridity and dark-mixed BSC cover, which is currently inferred to be statistically insignificant (Figure 4C). A general negative relationship between cover of this BSC group and aridity has also been well documented (Maestre and others 2015, 2021; Bowker and others 2016; Read and others 2016; Weber and others 2022). Marginal significance of the effect of aridity in our analysis may be caused by differential responses of constituents within dark-mixed BSCs, as lichens and mosses vary both in relative proportion and stress tolerance (Ferrenberg and others 2015; Bowker and others 2016). These results suggest that patches of light cyanobacteria-dominated crusts, with greater water stress tolerance and faster lateral expansion rate than dark-mixed BSCs (Sorochkina and others 2018; Becerra-Absalón and others 2019), can persist under increased aridity through the gradual modification of patch attributes and configuration. In contrast, patches of dark-mixed crusts, which have been shown to be more sensitive to climatic variation (Reed and others 2012; Maestre and others 2015; Rodríguez-Caballero and others 2022), may not sufficiently spatially adjust through regeneration, possibly resulting in reduced cover under increased stress—consistent with other studies (Reed and others 2012, 2019; Maestre and others 2015; Ferrenberg and others 2015; Rodríguez-Caballero and others 2018a).

Sensitive species constituting dark-mixed BSCs have been observed to rely significantly on the physical conditions of soil (Bowker and others 2016; Weber and others 2022). We found that coarser soil substrate likely increased the positive interaction between these BSCs and woody vegetation (Figure 5B) and plausibly reduced dark-mixed BSC cover (Figure 4C). Fine textured soil provides both high water holding capacity and nutrient availability for patches of sensitive dark-mixed BSCs (Bowker and others 2006; Bowker and Belnap 2008). Under coarser soil conditions, where cover of dark-mixed BSCs is often reduced (Weber and others 2022), these organisms likely have greater reliance on local stress amelioration by woody vegetation, which promote shading, relatively high soil moisture, and nutrient availability (Zhang and others 2016; Havrilla and others 2019). While, under this assumption, it is expected that aridity will increase the spatial aggregation of dark-mixed BSCs and woody vegetation, we found an insignificant negative effect of aridity on the strength of this generally positive interaction (Figure 5B). However, because our classifications did not consider dark-mixed BSCs directly under woody canopies, the actual association between these two groups in more arid sites might be slightly more positive than the level we quantified. While both dark-mixed and light cyanobacteria BSC patches can locally increase soil fineness through deposition (Belnap 2003), our soil texture data captured the mean state of a site and variation across sites, instead of within-site heterogeneity. We also found that soil calcareousness likely increased the spatial segregation between woody vegetation and dark-mixed BSCs (Figure 5B). We speculate that this is likely an effect of lichens. Abundant in calcareous and gypsum soils, where woody vegetation has difficulty establishing (Belnap and others 2001; Lalley and Viles 2008; Moya and others 2020), lichens can provide shade and habitat for other sensitive BSC constituents (Rosentreter and others 2016). Through increased local shading and soil moisture, lichen abundance in calcareous soils may provide functional redundancy at small scales for habitat otherwise provided by woody vegetation (Rosentreter and others 2016; Havrilla and others 2019). As the spatial interaction between BSC lichens and vegetation in drylands likely does not change with aridity (Navas Romero and others 2020), increased abundance of lichens within dark-mixed BSC patches may allow dark-mixed patches to persist under stress without relying on woody plants (Figure 5B). However, lichens are also notably susceptible to climate change and disturbance (Navas Romero and others 2020; Finger-Higgens and others 2022; Ladrón de Guevara and Maestre 2022). These results highlight that, in addition to climate, dark-mixed BSC patches are likely highly sensitive to local soil conditions—essentially binding them in space, and hence, resulting in a reduced capacity and likeli-

hood of patch adjustments in space under increased stress.

The negative effects of grazing on BSC communities are well documented, with grazing likely decreasing total cover and functional diversity of BSC communities and subsequently degrading ecosystem function (Soliveres and Eldridge 2020; Mallen-Cooper and others 2018; Root and others 2020; Chamizo and others 2016; Ding and Eldridge 2020). We found that grazing intensity at our study sites most significantly affected the patch complexity of light cyanobacteria BSCs, exhibiting a positive effect, rather than decreasing its cover (Figure 4A). We also found that grazing weakly decreased dark-mixed BSC cover (Figure 4C). This suggests that trampling fragmented light cyanobacteria BSCs, but that these BSCs were somewhat resilient to trampling overall at our study sites, whereas dark-mixed BSCs possibly could not persist under trampling activity. The suggested resilience of light cyanobacteria BSCs to grazing is not likely an effect of climatic conditions, where rainfall shortly after grazing has been suggested to promote recovery (Dojani and others 2011), as we do not observe a significant relationship between grazing intensity and climatic water deficit (CWD) at our study sites (Figure S12). Therefore, soil stability and promotion of runoff by light cyanobacteria BSCs may be sustained under moderate grazing activity. However, we expect that light cyanobacteria BSCs can only sustain grazing disturbance up to a certain threshold under favorable climatic conditions, beyond which their abundance would likely decrease and possibly collapse.

Facilitation by Light Cyanobacteria BSCs

Under increasing stress, biota can also persist through reaping the benefits of facilitative interactions among species (Kéfi and others 2016). Light cyanobacteria BSCs can promote local runoff generation by releasing exopolysaccharides (EPS), which creates a smooth soil surface and clogs soil pores (Chamizo and others 2016; Kidron and others 2020, 2022; Eldridge and others 2020, 2021), likely providing a critical source of runoff for downslope biota (Yair 2001; Rodríguez-Caballero and others 2018b; Eldridge and others 2020). EPS also likely promote water adsorption to sediment particles, possibly providing stored water for other biota (Kidron and others 2020). Our analysis corroborates these findings, showing significant effect of water stress on the spatial associations between light cyanobacteria and other functional groups in

the landscape. Aridity was shown to reduce the spatial segregation between woody vegetation and light cyanobacteria BSCs (Figure 5A). Similarly, enhanced runoff induced by increased slope within a certain range also possibly increased the spatial proximity of light cyanobacteria BSCs and woody plants, as slope showed the second greatest mean effect size on this interaction, albeit insignificantly (Figure 5A). This response is only likely within a range of increased slope before runoff begins to concentrate in rills and vascular plants can no longer effectively intercept runoff by reorganization, possibly explaining the insignificance of this effect in our analysis. These results suggest that, under increased water limitation, woody plants may grow in areas closer to light cyanobacteria patches and capture runoff more effectively. While light cyanobacteria patches may plausibly shift toward vegetation, this effect is less likely as vegetative cover often inhibits cyanobacteria through deposition of leaf litter (Zhang and others 2016; Lan and others 2021).

The spatial proximity of dark-mixed BSC patches to light cyanobacteria likely increases with increased slope (Figure 5C). As we find that dark-mixed BSCs may have a limited capacity to adjust patch attributes, we expect the spatial interaction between BSC patch types to increase with slope as dark-mixed BSCs most often develop within, or adjacent to, light cyanobacteria patches. Light cyanobacteria BSCs may develop into dark-mixed BSC patches at favorable microsites where runoff collects, and dark-mixed patches may return to a cyanobacteria-dominant state in unfavorable areas. The mean effect of increased aridity on the interaction between the two types of BSCs was less than that of slope and was insignificant, further suggesting patches of dark-mixed BSCs may have a limited capacity to spatially respond to increased climatic stress. Inciting such a patch-level response in runoff sinks of woody vegetation and dark-mixed BSCs suggests the significant role of light cyanobacteria BSCs in organizing the spatial structure of drylands and in affecting dryland ecosystem productivity through runoff–runon dynamics (Chamizo and others 2012a; Rodríguez-Caballero and others 2018b; Eldridge and others 2020).

Community Level Spatial Self-organization in Drylands

Biotic agents and their associated spatial feedbacks driven by resource redistribution create a dynamic ecohydrological matrix in drylands (Puigdefábregas

2005; Kéfi and others 2007; Belnap and others 2016). Through spatial self-organization and adjustment of spatial patterns over time, productivity may be maintained under a range of increased aridity (Bastiaansen and others 2018; Rietkerk and others 2021). In drylands, where abiotic stress is high and likely to increase in many regions, much attention has been given to their response to decreased water availability, considering only vascular plants (Rietkerk and others 2004, 2021; Pringle and Tarnita 2017; Bastiaansen and others 2018). However, our analysis suggests that BSCs, which often cover more area than vascular plants (Bowker and others 2018), may significantly drive the reorganization of biota in space through the redistribution of scarce water. Patch scale responses of light cyanobacteria BSCs (Figure 4A), an important source of runoff, to water limitation were paired with spatial adjustments in woody plants (Figure 5A), and to a limited extent, dark-mixed BSCs (Figure 5C). In dryland autotrophic communities, high tolerance of light cyanobacteria to stress may therefore act as a buffer for highly sensitive dark-mixed BSCs and vascular plants, which are often considered to be runoff sinks (Rodríguez-Caballero and others 2018b; Chen and others 2020). This coordination between multiple functional groups in dryland communities likely significantly affects ecosystem resilience, possibly delaying an abrupt loss in vegetation cover under increased aridity. Coupled, or mutually linked, spatial responses of BSCs and vascular plants to water limitation suggest that spatial self-organization in dryland ecosystems is likely a community-level response. While changes in ecosystem productivity may be dominated by changes in vascular plant cover, BSCs likely significantly alter responses and spatiotemporal dynamics of vascular plants in drylands.

While we found evidence of coupled patch responses of BSCs and vegetation to stress through observational data and correlations revealed by statistical models, controlled experimentation is necessary to fully elucidate mechanisms of patch responses and ecohydrological interactions. Future analysis is also necessary to relate species-level composition to functional BSC patch types as well as further characterize spatial responses of dark-mixed BSC patches. Contrasting patch responses of functionally unique biota within dark-mixed BSCs, such as lichens and mosses, may induce inconsistencies in the behavior of dark-mixed patches in aggregate. Consideration of species-level responses would also likely help elucidate processes driving community level self-organization in drylands. Such future studies would benefit from utilizing hyperspectral imagery, likely improving classification accuracies of BSC species (Baxter and others 2021). We also recommend future studies investigate the spatial relationships and dynamics between BSC patches and herbaceous vegetation. Ecohydrological dynamics associated with herbaceous vegetation could be distinctively different from woody plants and they likely play a key role in dryland ecosystems where grasses predominate.

CONCLUSIONS

Our results show that, like vascular plants, BSCs form patches in space that mediate and respond to the redistribution of scarce resources in drylands. Patches of light cyanobacteria BSCs can likely persist through gradual spatial alterations under stress, likely due to low water requirements and relatively fast dispersal and expansion rates. Alternatively, more sensitive patches of dark-mixed BSCs may have a limited capacity to adjust patch attributes to environmental conditions through regeneration, suggesting a relatively high likelihood of decline in their cover under increased stress. Varying species composition of dark-mixed patches, assemblages largely composed of lichens and bryophytes, may explain varying patch responses of these BSCs. Furthermore, spatial associations of patches of different biota also change with water availability. Light cyanobacteria BSC patches may act as significant sources of runoff for sensitive patches of vegetation and dark-mixed BSCs under high stress—possibly increasing dryland ecosystem resilience. Our study calls for a new paradigm of considering spatial self-organization in drylands through multiple interacting functional groups, instead of vascular plants only, to improve our predictive capacity of dryland response to global change.

DATA AVAILABILITY

REFERENCES

Abatzoglou JT, Dobrowski SZ, Parks SA, Hegewisch KC. 2018. TerraClimate, a high-resolution global dataset of monthly climate and climatic water balance from 1958–2015. Sci Data 5:170191.

Agisoft LLC. 2021. Agisoft metashape user manual: standard edition version 1.7. St. Petersburg: Agisoft LLC.

Aguiar MR, Sala OE. 1999. Patch structure, dynamics and implications for the functioning of arid ecosystems. Trends Ecol Evol 14(7):273–277.

Amir M-M, Ilan S, Shlomo S, Hiam A-G, Shimshon S, Zaady E. 2022. The dynamic of the eco-hydrological interrelations between shrubs and biocrusts in the Negev shrublands: empiric assessments and perspectives for shrubland rehabilitation. Catena 214:106296.

AOAC Official Method 972.43. 1997. Microchemical determination of carbon, hydrogen, and nitrogen, automated method. Official Methods of Analysis of AOAC International. 16th edition. Arlington: AOAC International. pp. 5–6.

Barger NN, Castle SC, Dean GN. 2013. Denitrification from nitrogen-fixing biologically crusted soils in a cool desert environment, southeast Utah, USA. Ecol Process 2:16.

Barger NN, Weber B, Garcia-Pichel F, Zaady E, Belnap J. 2016. Patterns and controls on nitrogen cycling of biological soil crusts. In: Weber B, Büdel B, Belnap J, Eds. Biological soil crusts: an organizing principle in drylands. Ecological studies. Vol. 226. Cham: Springer. pp 257–285.

Bastiaansen R, Jaïbi O, Deblauwe V, Eppinga MB, Siteur K, Siero E, Mermoz S, Bouvet A, Doelman A, Rietkerk M. 2018. Multistability of model and real dryland ecosystems through spatial self-organization. Proc Natl Acad Sci 115(44):11256–11261.

Baxter C, Mallen-Cooper M, Lyons MB, Cornwell WK. 2021. Measuring reflectance of tiny organisms: the promise of species level biocrust remote sensing. Methods Ecol Evol 12(11):2174–2183.

Becerra-Absalón I, Muñoz-Martín MÁ, Montejano G, Mateo P. 2019. Differences in the cyanobacterial community composition of biocrusts from the drylands of Central Mexico. Are there endemic species? Front Microbiol 10:937.

Belnap J. 2003. The world at your feet: desert biological soil crusts. Front Ecol Environ 1(4):181–189.

Belnap J, Büdel B. 2016. Biological soil crusts as soil stabilizers. In: Weber B, Büdel B, Belnap J, Eds. Biological soil crusts: an organizing principle in drylands. Ecological studies. Vol. 226. Cham: Springer. pp 305–320r.

Belnap J, Büdel B, Lange OL. 2001. Biological soil crusts: characteristics and distribution. In: Belnap J, Lange OL, Eds. Biological soil crusts: structure, function, and management ecological studies. Vol. 150. Berlin: Springer. pp 3–30.

Belnap J, Phillips SL, Witwicki DL, Miller ME. 2008. Visually assessing the level of development and soil surface stability of cyanobacterially dominated biological soil crusts. J Arid Environ 72(7):1257–1264.

Belnap J, Weber B, Büdel B. 2016. Biological soil crusts as an organizing principle in drylands. In: Weber B, Büdel B, Belnap J, Eds. Biological soil crusts: an organizing principle in drylands. Ecological studies. Vol. 226. Cham: Springer. pp 3–13.

Berdugo M, Delgado-Baquerizo M, Soliveres S, Hernández-Clemente R, Zhao Y, Gaitán JJ, Gross N, Saiz H, Maire V, Lehmann A, Rillig MC, Solé RV, Maestre FT. 2020. Global ecosystem thresholds driven by aridity. Science 367(6479):787–790.

Bowker MA, Belnap J. 2008. A simple classification of soil types as habitats of biological soil crusts on the Colorado Plateau, USA. J Veg Sci 19(6):831–840.

Bowker MA, Belnap J, Davidson DW, Goldstein H. 2006. Correlates of biological soil crust abundance across a continuum of spatial scales: support for a hierarchical conceptual model. J Appl Ecol 43(1):152–163.

Bowker MA, Eldridge DJ, Val J, Soliveres S. 2013. Hydrology in a patterned landscape is co-engineered by soil-disturbing animals and biological crusts. Soil Biol Biochem 61:14–22.

Bowker MA, Belnap J, Büdel B, Sannier C, Petrasiak N, Eldridge DJ, Rivera-Aguilar V. 2016. Controls on distribution patterns of biological soil crusts at micro- to global scales. In: Weber B, Büdel B, Belnap J, Eds. Biological soil crusts: an organizing principle in drylands. Ecological studies. Vol. 226. Cham: Springer. pp 173–179.

Bowker MA, Reed SC, Maestre FT, Eldridge DJ. 2018. Biocrusts: the living skin of the earth. Plant Soil 429:1–7.

Bro R, Smilde AK. 2014. Principal component analysis. Anal Methods 6:2812–2831.

Bryce S, Strittholt J, Ward B, Bachelet D. 2012. Colorado Plateau rapid ecoregional assessment report. Denver: U.S. Department of Interior Bureau of Land Management.

Büdel B, Dulić T, Darienko T, Rybalka N, Friedl T. 2016. Cyanobacteria and algae of biological soil crusts. In: Weber B, Büdel B, Belnap J, Eds. Biological soil crusts: an organizing principle in drylands. Ecological studies. Vol. 226. Cham: Springer. pp 55–80.

Cantón Y, Chamizo S, Rodriguez-Caballero E, Lázaro R, Roncero-Ramos B, Román JR, Solé-Benet A. 2020. Water regulation in cyanobacterial biocrusts from drylands: negative impacts of anthropogenic disturbance. Water 12(3):720.

Chamizo S, Stevens A, Cantón Y, Miralles I, Domingo F, van Wesemael B. 2012a. Discriminating soil crust type, development stage and degree of disturbance in semiarid environments from their spectral characteristics. Eur J Soil Sci 63:42–53.

Chamizo S, Cantón Y, Rodríguez-Caballero E, Domingo F, Escudero A. 2012b. Runoff at contrasting scales in a semiarid ecosystem: a complex balance between biological soil crust features and rainfall characteristics. J Hydrol 452–453:130–138.

Chamizo S, Belnap J, Eldridge DJ, Cantón Y, Malam Issa O. 2016. The role of biocrusts in arid land hydrology. In: Weber B, Büdel B, Belnap J, Eds. Biological soil crusts: an organizing principle in drylands. Ecological studies. Vol. 226. Cham: Springer. pp 321–346.

Chen N, Yu K, Jia R, Teng J, Zhao C. 2020. Biocrust as one of multiple stable states in global drylands. Sci Adv 6(39):eaay3763.

Colica G, Li H, Rossi F, Li D, Liu Y, de Philippis R. 2014. Microbial secreted exopolysaccharides affect the hydrological

behavior of induced biological soil crusts in desert sandy soils. Soil Biol Biochem 68:62–70.

Cook BI, Mankin JS, Marvel K, Williams AP, Smerdon JE, Anchukaitis KJ. 2020. Twenty-First Century drought projections in the CMIP6 forcing scenarios. Earth's Future 8(6):e2019EF001461.

Couteron P, Anthelme F, Clerc M, Escaff D, Fernandez-Oto C, Tlidi M. 2014. Plant clonal morphologies and spatial patterns as self-organized responses to resource-limited environments. Philos Trans R Soc A Math Phys Eng Sci 372:20140102.

D'Odorico P, Caylor K, Okin GS, Scanlon TM. 2007. On On soil moisture–vegetation feedbacks and their possible effects on the dynamics of dryland ecosystems. J Geophys Res Biogeosci 112(G4):1–10.

Deblauwe V, Couteron P, Lejeune O, Bogaert J, Barbier N. 2011. Environmental modulation of self-organized periodic vegetation patterns in Sudan. Ecography 34:990–1001.

Deblauwe V, Couteron P, Bogaert J, Barbier N. 2012. Determinants and dynamics of banded vegetation pattern migration in arid climates. Ecol Monogr 82:3–21.

Demšar U, Harris P, Brunsdon C, Fotheringham AS, McLoone S. 2013. Principal component analysis on Spatial Data: An overview. Ann Assoc Am Geogr 103(1):106–128.

Ding J, Eldridge DJ. 2020. Biotic and abiotic effects on biocrust cover vary with microsite along an extensive aridity gradient. Plant Soil 450:429–441.

Dojani S, Büdel B, Deutschewitz K, Weber B. 2011. Rapid succession of biological soil crusts after experimental disturbance in the Succulent Karoo, South Africa. Appl Soil Ecol 48(3):263–269.

Duniway MC, Nauman TW, Johanson JK, Green S, Miller ME, Williamson JC, Bestelmeyer BT. 2016. Generalizing ecological site concepts of the colorado plateau for landscape-level applications. Rangelands 38(6):342–349.

Eidenshink J, Schwind B, Brewer K, Zhu ZL, Quayle B, Howard S. 2007. A project for monitoring trends in burn severity. Fire Ecol 3(1):3–21.

Eldridge DJ, Zaady E, Shachak M. 2000. Infiltration through three contrasting biological soil crusts in patterned landscapes in the Negev, Israel. Catena 40(3):323–336.

Eldridge DJ, Reed SC, Travers SK, Bowker MA, Maestre FT, Ding J, Havrilla CA, Rodriguez-Caballero E, Barger NN, Weber B, Antoninka A, Belnap J, Chaudhary B, Faist A, Ferrenberg S, Huber-Sannwald E, Malam Issa O, Zhao Y. 2020. The pervasive and multifaceted influence of biocrusts on water in the world's drylands. Glob Change Biol 26(10):6003–6014.

Eldridge DJ, Mallen-Cooper M, Ding J. 2021. Biocrust functional traits reinforce runon-runoff patchiness in drylands. Geoderma 400:115152.

Exelis Visual Information Solutions. 2022. Maximum likelihood. Boulder: Exelis Visual Information Solutions ENVI 5.5.

Ferrenberg S, Reed SC, Belnap J. 2015. Climate change and physical disturbance cause similar community shifts in biological soil crusts. Proc Natl Acad Sci 112(39):12116–12121.

Fetzel T, Havlik P, Herrero M, Erb K. 2017. Seasonality constraints to livestock grazing intensity. Glob Change Biol 23(4):1636–1647.

Finger-Higgens R, Duniway MC, Fick S, Geiger EL, Hoover DL, Pfennigwerth AA, van Scyoc MW, Belnap J. 2022. Decline in biological soil crust N-fixing lichens linked to increasing summertime temperatures. Proc Natl Acad Sci 119(16):e2120975119.

Fitzgerald RW, Lees BG. 1994. Assessing the classification accuracy of multisource remote sensing data. Remote Sens Environ 47(3):362–368.

Gelman A, Shalizi CR. 2013. Philosophy and the practice of Bayesian statistics. Br J Math Stat Psychol 66:8–38.

Gelman A, Lee D, Guo J. 2015. Stan: a probabilistic programming language for Bayesian inference and optimization. J Educ Behav Stat 40(5):530–543.

Gorelick N, Hancher M, Dixon M, Ilyushenko S, Thau D, Moore R. 2017. Google earth engine: planetary-scale geospatial analysis for everyone. Remote Sens Environ 202:18–27.

Guan H, Liu X. 2019. Does biocrust successional stage determine the degradation of vascular vegetation via alterations in its hydrological roles in semi-arid ecosystem? Ecohydrology 12(3):e2075.

Havrilla CA, Barger NN. 2018. Biocrusts and their disturbance mediate the recruitment of native and exotic grasses from a hot desert ecosystem. Ecosphere 9(7):e02361.

Havrilla CA, Chaudhary VB, Ferrenberg S, Antoninka AJ, Belnap J, Bowker MA, Eldridge DJ, Faist AM, Huber-Sannwald E, Leslie AD, Rodriguez-Caballero E, Zhang Y, Barger NN. 2019. Towards a predictive framework for biocrust mediation of plant performance: a meta-analysis. J Ecol 107(6):2789–2807.

Havrilla CA, Villarreal ML, DiBiase JL, Duniway MC, Barger NN. 2020. Ultra-high-resolution mapping of biocrusts with unmanned aerial systems. Remote Sens Ecol Conserv 6(4):441–456.

Hesselbarth MHK, Sciaini M, With KA, Wiegand K, Nowosad J. 2019. landscapemetrics: an open-source R tool to calculate landscape metrics. Ecography 42:1648–1657.

Kéfi S, Rietkerk M, van Baalen M, Loreau M. 2007. Local facilitation, bistability and transitions in arid ecosystems. Theor Popul Biol 71(3):367–379.

Kéfi S, Holmgren M, Scheffer M. 2016. When can positive interactions cause alternative stable states in ecosystems? Funct Ecol 30(1):88–97.

Kidron GJ. 2007. Millimeter-scale microrelief affecting runoff yield over microbiotic crust in the Negev Desert. Catena 70(2):266–273.

Kidron GJ. 2019. Biocrust research: a critical view on eight common hydrological-related paradigms and dubious theses. Ecohydrology 12(2):e2061.

Kidron GJ, Wang Y, Herzberg M. 2020. Exopolysaccharides may increase biocrust rigidity and induce runoff generation. J Hydrol 588:125081.

Kidron GJ, Lichner L, Fischer T, Starinsky A, Or D. 2022. Mechanisms for biocrust-modulated runoff generation—a review. Earth-Sci Rev 231:104100.

Ladrón de Guevara M, Maestre FT. 2022. Ecology and responses to climate change of biocrust-forming mosses in drylands. J Exp Bot 73(13):4380–4395.

Lalley JS, Viles HA. 2008. Recovery of lichen-dominated soil crusts in a hyper-arid desert. Biodivers Conserv 17:1–20.

Lan S, Thomas AD, Tooth S, Wu L, Elliott DR. 2021. Effects of vegetation on bacterial communities, carbon and nitrogen in dryland soil surfaces: implications for shrub encroachment in the southwest Kalahari. Sci Total Environ 764:142847.

Lange OL, Belnap J. 2016. How biological soil crusts became recognized as a functional unit: a selective history. In: Weber B, Büdel B, Belnap J, Eds. Biological soil crusts: an organizing principle in drylands. Ecological studies. Vol. 226. Cham: Springer. pp 15–33.

Larsen LG, Choi J, Nungesser MK, Harvey JW. 2012. Directional connectivity in hydrology and ecology. Ecol Appl 22(8):2204–2220.

Larson JE, Funk JL. 2016. Seedling root responses to soil moisture and the identification of a belowground trait spectrum across three growth forms. New Phytol 210(3):827–838.

Lian X, Piao S, Chen A, Huntingford C, Fu B, Li LZX, Huang J, Sheffield J, Berg AM, Keenan TF, McVicar TR, Wada Y, Wang X, Wang T, Yang Y, Roderick ML. 2021. Multifaceted characteristics of dryland aridity changes in a warming world. Nat Rev Earth Environ 2:232–250.

Maestre FT, Escolar C, Bardgett RD, Dungait JAJ, Gozalo B, Ochoa V. 2015. Warming reduces the cover and diversity of biocrust-forming mosses and lichens, and increases the physiological stress of soil microbial communities in a semi-arid Pinus halepensis plantation. Front Microbiol 6:865.

Maestre FT, Benito BM, Berdugo M, Concostrina-Zubiri L, Delgado-Baquerizo M, Eldridge DJ, Guirado E, Gross N, Kéfi S, le Bagousse-Pinguet Y, Ochoa-Hueso R, Soliveres S. 2021. Biogeography of global drylands. New Phytol 231:540–558.

Maier S, Tamm A, Wu D, Caesar J, Grube M, Weber B. 2018. Photoautotrophic organisms control microbial abundance, diversity, and physiology in different types of biological soil crusts. ISME J 12:1032–1046.

Mallen-Cooper M, Eldridge DJ, Delgado-Baquerizo M. 2018. Livestock grazing and aridity reduce the functional diversity of biocrusts. Plant Soil 429:175–185.

Mayor AG, Bautista S, Rodriguez F, Kéfi S. 2019. Connectivity-mediated ecohydrological feedbacks and regime shifts in drylands. Ecosystems 22:1497–1511.

McGarigal K, Marks, B. 1995. FRAGSTATS: spatial pattern analysis program for quantifying landscape structure. Gen. Tech. Rep. PNW-GTR-351. Portland, OR: U.S. Department of Agriculture, Forest Service, Pacific Northwest Research Station. pp 122.

McIntyre C, Archer SR, Predick KI, Belnap J. 2021. Biocrusts do not differentially influence emergence and early establishment of native and non-native grasses. Ecosphere 12(12):e03841.

Moya P, Molins A, Chiva S, Bastida J, Barreno E. 2020. Symbiotic microalgal diversity within lichenicolous lichens and crustose hosts on Iberian Peninsula gypsum biocrusts. Sci Rep 10:14060.

Muñoz-Martín MÁ, Becerra-Absalón I, Perona E, Fernández-Valbuena L, Garcia-Pichel F, Mateo P. 2019. Cyanobacterial biocrust diversity in Mediterranean ecosystems along a latitudinal and climatic gradient. New Phytol 221:123–141.

Navas Romero AL, Herrera Moratta MA, Martinez Carretero E, Rodriguez RA, Vento B. 2020. Spatial distribution of biological soil crusts along an aridity gradient in the central-west of Argentina. J Arid Environ 176:104099.

Okin GS, Heras MM, Saco PM, Throop HL, Vivoni ER, Parsons AJ, Wainwright J, Peters DP. 2015. Connectivity in dryland landscapes: shifting concepts of spatial interactions. Front Ecol Environ 13(1):20–27.

Perry JN. 1998. Measures of spatial pattern for counts. Ecology 79(3):1008–1017.

Perry JN, Dixon PM. 2002. A new method to measure spatial association for ecological count data. Écoscience 9(2):133–141.

Perry JN, Winder L, Holland JM, Alston RD. 1999. Red-blue plots for detecting clusters in count data. Ecol Lett 2(2):106–113.

Petz K, Alkemade R, Bakkenes M, Schulp CJE, van der Velde M, Leemans R. 2014. Mapping and modelling trade-offs and synergies between grazing intensity and ecosystem services in rangelands using global-scale datasets and models. Glob Environ Change 29:223–234.

Pringle RM, Tarnita CE. 2017. Spatial self-organization of ecosystems: integrating multiple mechanisms of regular-pattern formation. Ann Rev Entomol 62:359–377.

Puigdefábregas J. 2005. The role of vegetation patterns in structuring runoff and sediment fluxes in drylands. Earth Surf Process Landf 30(2):133–147.

Read CF, Elith J, Vesk PA. 2016. Testing a model of biological soil crust succession. J Veg Sci 27:176–186.

Reed SC, Coe KK, Sparks JP, Housman DC, Zelikova TJ, Belnap J. 2012. Changes to dryland rainfall result in rapid moss mortality and altered soil fertility. Nat Clim Change 2:752–755.

Reed SC, Delgado-Baquerizo M, Ferrenberg S. 2019. Biocrust science and global change. N Phytol 223(3):1047–1051.

Rietkerk M, Dekker SC, de Ruiter PC, van de Koppel J. 2004. Self-organized patchiness and catastrophic shifts in ecosystems. Science 305(5692):1926–1929.

Rietkerk M, Bastiaansen R, Banerjee S, van de Koppel J, Baudena M, Doelman A. 2021. Evasion of tipping in complex systems through spatial pattern formation. Science 374(6564):eabj0359.

Rodríguez-Caballero E, Cantón Y, Chamizo S, Afana A, Solé-Benet A. 2012. Effects of biological soil crusts on surface roughness and implications for runoff and erosion. Geomorphology 145–146:81–89.

Rodríguez-Caballero E, Paul M, Tamm A, Caesar J, Büdel B, Escribano P, Hill J, Weber B. 2017. Biomass assessment of microbial surface communities by means of hyperspectral remote sensing data. Sci Total Environ 586:1287–1297.

Rodríguez-Caballero E, Belnap J, Büdel B, Crutzen PJ, Andreae MO, Pöschl U, Weber B. 2018a. Dryland photoautotrophic soil surface communities endangered by global change. Nat Geosci 11(3):185–189.

Rodríguez-Caballero E, Chamizo S, Roncero-Ramos B, Román R, Cantón Y. 2018b. Runoff from biocrust: a vital resource for vegetation performance on Mediterranean steppes. Ecohydrology 11(6):e1977.

Rodríguez-Caballero E, Román JR, Chamizo S, Roncero Ramos B, Cantón Y. 2019. Biocrust landscape-scale spatial distribution is strongly controlled by terrain attributes: topographic thresholds for colonization in a semiarid badland system. Earth Surf Process Landf 44:2771–2779.

Rodríguez-Caballero E, Reyes A, Kratz A, Caesar J, Guirado E, Schmiedel U, Weber B. 2022. Effects of climate change and land use intensification on regional biological soil crust cover and composition in Southern Africa. Geoderma 406:115508.

Root HT, Miller JED, Rosentreter R. 2020. Grazing disturbance promotes exotic annual grasses by degrading soil biocrust communities. Ecol Appl 30(1):e02016.

Rosentreter R, Bowker MA, Belnap J. 2007. A field guide to biological soil crusts of western U.S. drylands: common lichens and bryophytes. Denver: U.S. Government Publishing Office.

Rosentreter R, Eldridge DJ, Westberg M, Williams L, Grube M. 2016. Structure, composition, and function of biocrust lichen communities. In: Weber B, Büdel B, Belnap J, Eds. Biological soil crusts: an organizing principle in drylands. Ecological studies. Vol. 226. Cham: Springer. pp 121–138.

Rozenstein O, Adamowski J. 2017. A review of progress in identifying and characterizing biocrusts using proximal and remote sensing. Int J Appl Earth Obs Geoinf 57:245–255.

Sanchez-Martinez P, Martínez-Vilalta J, Dexter KG, Segovia RA, Mencuccini M. 2020. Adaptation and coordinated evolution of plant hydraulic traits. Ecol Lett 23(11):1599–1610.

Scheffer M. 2009. Critical transitions in nature and society. Princeton: Princeton University Press. p 400.

Sheldrick BH, Wang C. 1993. Particle size analysis. In: Carter MR, Ed. Soil sampling and methods of analysis, . Boca Raton: Lewis Publishers. pp 499–517.

Shutaywi M, Kachouie NN. 2021. Silhouette analysis for performance evaluation in machine learning with applications to clustering. Entropy 23(6):759.

Snyder K, Huntington J, Wehan B, Morton C, Stringham T. 2019. Comparison of landsat and land-based phenology camera normalized difference vegetation index (NDVI) for dominant plant communities in the great basin. Sensors 19(5):1139.

Soliveres S, Eldridge DJ. 2020. Dual community assembly processes in dryland biocrust communities. Funct Ecol 34(4):877–887.

Sorochkina K, Velasco Ayuso S, Garcia-Pichel F. 2018. Establishing rates of lateral expansion of cyanobacterial biological soil crusts for optimal restoration. Plant Soil 429:199–211.

Svensson JR, Marshall DJ. 2015. Limiting resources in sessile systems: food enhances diversity and growth of suspension feeders despite available space. Ecology 96(3):819–827.

Tamm A, Caesar J, Kunz N, Colesie C, Reichenberger H, Weber B. 2018. Ecophysiological properties of three biological soil crust types and their photoautotrophs from the Succulent Karoo, South Africa. Plant Soil 429:127–146.

Taubner H, Roth B, Tippkötter R. 2009. Determination of soil texture: comparison of the sedimentation method and the laser-diffraction analysis. J Plant Nutr Soil Sci 172(2):161–171.

Thorne RF. 1986. A historical sketch of the vegetation of the mojave and colorado deserts of the American Southwest. Ann Missouri Bot Gard 73:642–651.

Tilman D. 1982. Resource competition and community structure (MPB-17). Vol. 17. Princeton: Princeton University Press. p 296.

U.S. Geological Survey. 2022. 3D elevation program 10-meter resolution digital elevation model.

U.S. Salinity Laboratory Staff. 1954. Alkaline-earth carbonates by gravimetric loss of carbon dioxide. In: Diagnosis and improvement of saline and alkali soils. USDA Agricultural Handbook. Washington, D.C.: U.S. Government Printing Office, pp 105.

van de Koppel J, Rietkerk M. 2004. Spatial interactions and resilience in arid ecosystems. Am Nat 163:113–121.

von Hardenberg J, Kletter AY, Yizhaq H, Nathan J, Meron E. 2010. Periodic versus scale-free patterns in dryland vegetation. Proc R Soc B Biol Sci 277(1688):1771–1776.

Wang L, Manzoni S, Ravi S, Riveros-Iregui D, Caylor K. 2015. Dynamic interactions of ecohydrological and biogeochemical processes in water-limited systems. Ecosphere 6(8):133.

Weber B, Hill J. 2016. Remote sensing of biological soil crusts at different scales. In: Weber B, Büdel B, Belnap J, Eds. Biological soil crusts: an organizing principle in drylands. Ecological studies. Vol. 226. Cham: Springer. pp 215–234.

Weber B, Wu D, Tamm A, Ruckteschler N, Rodríguez-Caballero E, Steinkamp J, Meusel H, Elbert W, Behrendt T, Sörgel M, Cheng Y, Crutzen PJ, Su H, Pöschl U. 2015. Biological soil crusts accelerate the nitrogen cycle through large NO and HONO emissions in drylands. Proc Natl Acad Sci USA 112(50):15384–15389.

Weber B, Belnap J, Büdel B, Antoninka AJ, Barger NN, Chaudhary VB, Darrouzet-Nardi A, Eldridge DJ, Faist AM, Ferrenberg S, Havrilla CA, Huber-Sannwald E, Malam Issa O, Maestre FT, Reed SC, Rodriguez-Caballero E, Tucker C, Young KE, Zhang Y, Zhao Y, Zhou X, Bowker MA. 2022. What is a biocrust? A refined, contemporary definition for a broadening research community. Biol Rev 97(5):1768–1785.

Williams AJ, Buck BJ, Beyene MA. 2012. Biological soil crusts in the Mojave Desert, USA: micromorphology and pedogenesis. Soil Sci Soc Am J 76(5):1685–1695.

Yair A. 2001. Effects of biological soil crusts on water redistribution in the Negev Desert, Israel: a case study in longitudinal dunes. In: Belnap J, Lange OL, Eds. Biological soil crusts: structure, function, and management ecological studies. Vol. 150. Berlin, Heidelberg: Springer. pp 303–314.

Zhang Y, Aradottir AL, Serpe M, Boeken B. 2016. Interactions of biological soil crusts with vascular plants. In: Weber B, Büdel B, Belnap J, Eds. Biological soil crusts: an organizing principle in drylands. Ecological studies. Vol. 226. Cham: Springer. pp 385–406.